Droplet Growth by Coalescence in Binary Fluid Mixtures

Brian E. Burkhart,[1] Prasad V. Gopalkrishnan,[1] Steven D. Hudson,[1,2,*] and Alex M. Jamieson[1]
[1]*Department of Macromolecular Science, Case Western Reserve University, Cleveland, Ohio 44106-7202*
[2]*Polymers Division, National Institute of Standards and Technology, Gaithersburg, Maryland 20899-8544*

Michael A. Rother and Robert H. Davis
Department of Chemical Engineering, University of Colorado, Boulder, Colorado 80309-0424
(Received 14 March 2001; published 14 August 2001)

The evolution of the drop-size distribution in immiscible fluid mixtures following well-specified shear histories is investigated by *in situ* microscopy, allowing determination of the shear-induced coalescence efficiency ε. At small capillary number Ca, ε is constant, whereas at larger values of Ca, ε decreases, in agreement with theory accounting for slight deformation of the drops in close approach. Coalescence causes the drop-size distribution to broaden in general, but greater deformation of the larger drops at high shear rates causes the drop-size distribution to remain narrow.

DOI: 10.1103/PhysRevLett.87.098304 PACS numbers: 82.70.Kj

The properties of immiscible fluids (e.g., the texture of foods and the mechanical properties of polymer blends) depend strongly on the size of the dispersed phase. Usually the desired size is much smaller than the equilibrium size, so that small drops grow with time, primarily by coalescence, which requires the movement of drops toward one another. Although drop motion can occur by various means, an applied shear strain in the present experiments overwhelms both Brownian motion [1] and buoyancy [2,3] as the source of collisions.

A theoretical description of shear-induced (or orthokinetic) coalescence was first developed by Smoluchowski [4]. Neglecting droplet interactions, the frequency of droplet collisions and the concomitant growth of size can be calculated easily. Assuming that the drops are of equal radius a,

$$d[\ln(a)]/d\gamma = \phi(4/\pi)(2 - 2^{2/3})\varepsilon\,, \qquad (1)$$

where ϕ is the local volume fraction of the dispersed phase and γ is the shear strain. ε represents the coalescence efficiency, a correction to the original theory [5]. When ε is constant, the drop size grows exponentially with shear strain. Determination of ε is then simple, being derived directly from the slope of $\ln(a)$ vs γ [6–8].

Recent predictions of ε take into account droplet interactions. In particular, the trajectory analyses [9,10] used to compare the present experiments with theory follow the motion of pairs of drops by accounting for hydrodynamic interactions and van der Waals attractions. Coalescence is assumed when the attraction pulls the surfaces of the two drops into contact so that film rupture occurs. When the shear flow causes the drops to become close altogether, the pressure that builds up in the lubrication film between the drops causes their interfaces to become flattened or dimpled in the region of near contact. When attractions become dominant before flattening (i.e., for very small values of the ratio Ca/δ, where Ca is the capillary number, and δ is the dimensionless Hamaker parameter [11]), ε is essentially that of spherical drops [9]. ($\mathrm{Ca} = a\eta_c\dot{\gamma}/\sigma$, where $\dot{\gamma}$ is the shear rate, σ is the interfacial tension, and δ represents the ratio of attractive van der Waals forces to lubrication forces.) In this limit, ε depends primarily on the viscosity ratio ($p = \eta_d/\eta_c$) and the size ratio for a pair of drops ($k = a_1/a_2$, defined to be less than or equal to 1), and only weakly on attractive molecular forces. On the other hand, when flattening occurs before the interfaces are sufficiently close that attractions become important (i.e., for larger Ca/δ), ε is much lower than that of spherical drops, due to the slow film draining process [10].

In this Letter, we investigate the orthokinetic coalescence efficiency as a function of shear rate and temperature, and we compare drop-size distributions as a function of the degree of drop deformation. The two fluids used in this study are poly(ethylene glycol), PEG (the continuous phase), and poly(propylene glycol) PPG, the droplet phase. Their number-average molecular weights are $M_n = 10\,000$ and $12\,200$, respectively. The polydispersity of molecular weight for each is approximately $M_w/M_n = 1.1$, where M_w is the mass-averaged molecular weight, as determined by MALDI mass spectroscopy. Their individual viscosities (Table I) were measured using a Carrimed cone-and-plate rheometer and found to be Newtonian up to shear rates of at least $800\ \mathrm{s}^{-1}$. The interfacial tension between the two fluids (Table I) was measured by the droplet retraction technique [12] at temperatures of 75, 90, and 125 °C; isolated drops having a diameter ranging from

TABLE I. PEG viscosity, PPG viscosity, and interfacial tension.

T (°C)	η_c, PEG (Pa s)	η_d, PPG (Pa s)	σ (mN/m)
75	4.2	0.71	3.5
90	2.5	0.50	3.0
125	1.2[a]	0.24[a]	2.3

[a]Extrapolated based on an Arrhenius fit.

200 to 280 μm were investigated using a gap spacing of 500 μm. Ring tensiometry [13] was also performed, yielding similar results. Because of the chemical similarity of PEG and PPG, σ is relatively small, and any impurities are not likely to be surface active. Thus, this blend is appropriate for comparison with theories for binary fluids. Mixtures containing surfactants are also being studied [8].

Mixtures were examined with monochromatic light by bright-field or phase-contrast optical microscopy using a Linkam Scientific Instruments CSS-450 heated shearing cell mounted on an Olympus microscope equipped with a 20× long-working-distance objective and a (640 × 680 pixel) CCD camera. The image magnification (0.811 μm/pixel) was determined using a calibrated ruling. The shear cell has a parallel-plate geometry, in which one quartz disk is rotated relative to another. The smaller disk has a radius of 15 mm, and the observation window is situated at a radius of 7.5 mm, so that the shear field is relatively uniform (i.e., ±3%) throughout the 0.52 mm wide field of view. All shear rates are reported at the location of the center of the window.

Coalescence experiments were carried out at gap spacings of 50, 100, and 200 μm, and at temperatures of 75, 90, and 125 ± 0.1 °C. The mixture was first sheared at a high rate (e.g., 400 s^{-1}) to produce a relatively narrow distribution of small drops. Even at these rates, the Reynolds number $\mathrm{Re} = \rho\dot{\gamma}4h^2/\eta_c$ ($\rho \equiv$ density, $h \equiv$ half gap spacing) is small ($\sim 3 \times 10^{-3}$), so that Stokes flow can be assumed. After more than 1 min of preshear, the shear rate was decreased abruptly. In some instances, the bulk fluid drifted slightly for a few seconds following the step down. When this drift occurred, the system was observed carefully to ensure that no significant coalescence took place during this time.

A series of images was recorded during shear at regular intervals of strain. The beginning of the series was timed such that the first one or two images were during rapid shear, so that the beginning of slow shear could be determined. The drop-size distribution was measured from the images with an image analysis routine using the Danielson or circles operator [14], which fits a binary thresholded image with circular domains (Fig. 1). During slow shear, Ca is small enough (<0.1) that the drops are nearly spherical (Fig. 1). Mixtures having up to 10% dispersed phase could be investigated quantitatively, and number and volume average drop radii were calculated:

$$a_n = \sum_{i=1}^{n} n_i a_i \Big/ \sum_{i=1}^{n} n_i, \qquad a_v = \sum_{i=1}^{n} n_i a_i^4 \Big/ \sum_{i=1}^{n} n_i a_i^3 . \tag{2}$$

The total number of drops counted per image is approximately 500 to 3000. When the distribution of drop sizes is broad (as in Fig. 1), the value of a_v is more reliable than a_n, because analysis of the larger drops is more accurate.

Because the gap spacing is narrow, wall effects are significant and are treated as follows. When a fluid mixture is sheared, drops migrate away from a wall with a velocity

$$u_{\mathrm{mig}} = \left(\frac{3}{8}\right)\left(\frac{35}{32}\right)\frac{\sigma}{\eta}\,\mathrm{Ca}^2\left(\frac{a}{y_1}\right)^2, \tag{3}$$

where y_1 is the distance from the wall [15]. Moreover, droplet collisions induce random displacements parallel to the shear gradient, giving rise to a shear-induced self-diffusion coefficient:

$$D_{\mathrm{self}} = \phi\dot{\gamma}a^2 f_y , \tag{4}$$

where f_y is a coefficient that depends on Ca and p [16]. The diffusivity in a concentration gradient is larger than the self-diffusivity [17], and we use $D \approx 2D_{\mathrm{self}}$. At steady state, fluxes associated with these phenomena balance and the following volume fraction profile [18] is obtained:

$$\phi(y') = \phi_0 - \left(\frac{3}{8}\right)\left(\frac{35}{32}\right)\frac{1}{f_y}\,\mathrm{Ca}\left(\frac{a}{h}\right)\frac{1}{1 - y'^2}, \tag{5}$$

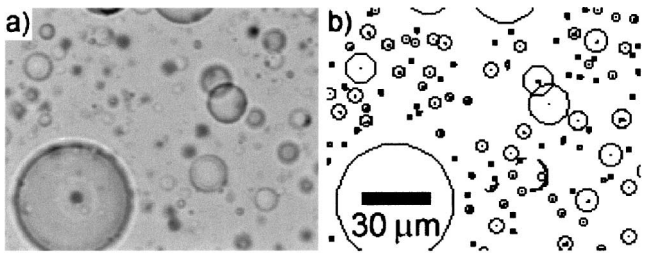

FIG. 1. A cropped portion of an (a) original bright-field and (b) processed image. The circles operator is able to resolve partially overlapped drops, as shown.

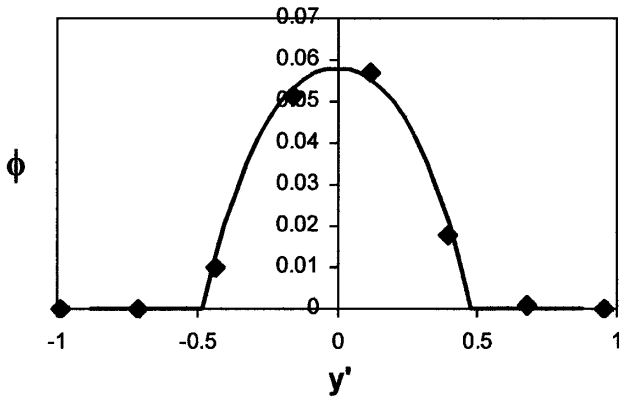

FIG. 2. The steady-state local volume fraction profile resulting from the balance of shear-induced diffusion and wall migration. The curve is calculated from Eq. (5) for the following experimental conditions: $\langle\phi\rangle = 0.022$, $R = 6.0$ μm, $h = 50$ μm, $\mathrm{Ca} = 0.40$, and $p = 0.2$ ($f_y = 0.05$, as determined from Ref. [16]), and the symbols represent experimental data. The mixture was sheared at 90 °C, first at 2 s^{-1} for 2 min to produce large drops and then at 80 s^{-1} for 11 min to achieve a narrow distribution of drops having a radius of 6.0 μm (Ca = 0.40, see Table I). The local concentration ϕ was assumed to be proportional to the number of drops, which was determined immediately after cessation of flow by adjusting the plane of focus at eight different positions within the gap and counting the number of drops in focus at each position y'.

TABLE II. Effective volume fractions for experiments[a] reported in Fig. 3.

$2h$ (μm)	$\langle\phi\rangle$	ϕ_{eff}
100	0.022	0.046
50	0.044	0.089
50	0.055	0.105
100	0.055	0.090
200	0.055	0.079
50	0.110	0.176

[a]Ca = 0.5, $p = 0.2$, $f_y = 0.05$ (see Ref. [16]), and $a = 1.7$ μm.

consistent with experimental data (Fig. 2). Since the volume fraction must be positive or zero, $\phi(y')$ is set to 0 if the above expression gives a negative value (i.e., near the wall). ϕ_0 is an integration constant determined by conservation of the total volume fraction, and $y' = y/h$, where $y = 0$ is the center plane of the cell and the bounding walls are at $y = \pm h$. Thus the local concentration ϕ of drops is greater near the center of the gap, causing coalescence to be more rapid in that region. Note that 3D behavior is preserved, because the drops are small compared to the width of the concentrated region.

For the experiments reported here, wall migration and shear-induced diffusion are only significant during the rapid preshear period. After a step down in rate, the shear rate and Ca are so small that both wall migration and shear-induced diffusion are insignificant. Therefore the volume fraction profile is essentially static but nonuniform during the coalescence period [18]. To understand the effect of this spatial distribution of drops, we recall that coalescence of moderately dilute suspensions involves collisions between pairs of drops, and that the collision frequency per unit volume is proportional to ϕ^2. Therefore, integrating Eq. (1) weighted by the local concentration ϕ, the effective concentration to leading order is

$$\phi_{\text{eff}} = \frac{\langle\phi^2\rangle}{\langle\phi\rangle}. \tag{6}$$

Table II lists values of ϕ_{eff} appropriate to experiments reported here. The ratio $\phi_{\text{eff}}/\langle\phi\rangle$ is a significant factor not considered in our earlier work [8], so that the values of ε reported then were higher than expected.

Growth of the volume averaged drop diameter $D_v = 2a_v$ as a function of increasing dimensionless time $\dot{\gamma}t\phi_{\text{eff}}$ is plotted in Fig. 3 for several shear rates, gap spacings, and dispersed phase volume fractions. For each shear rate, ε is initially constant, with a value of 0.56 (Fig. 3), and D_v grows exponentially as predicted by Eq. (1), suggesting that the effect of drop deformation is negligible for

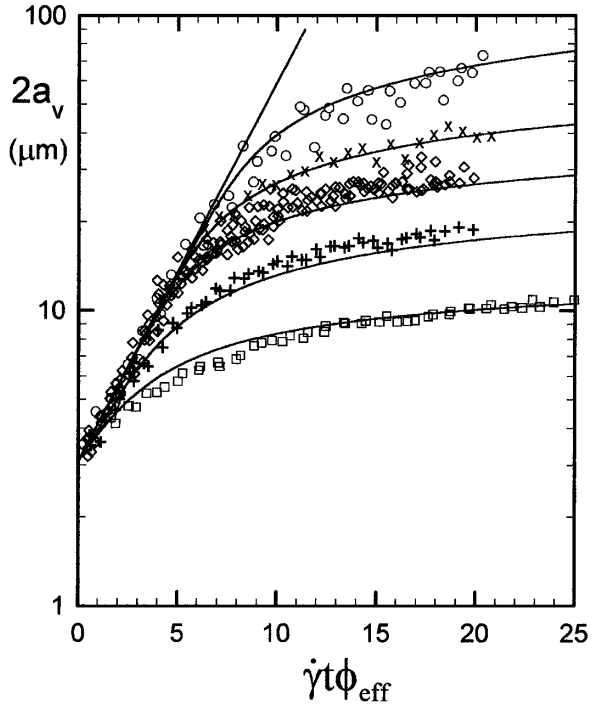

FIG. 3. Growth of the volume averaged drop diameter with increasing dimensionless time for mixtures of PPG in PEG at 90 °C. The curves represent a fit by a trajectory theory for deformable drops [10] with shear rates of 2, 5, 10, 20, and 50 s^{-1} from top to bottom, while the straight line is the prediction for spherical drops [9]. The data for 10 s^{-1} are for each of the experimental conditions (gap spacing and drop concentrations, and effective concentration) listed in Table II. For the other shear rates, two data sets are shown.

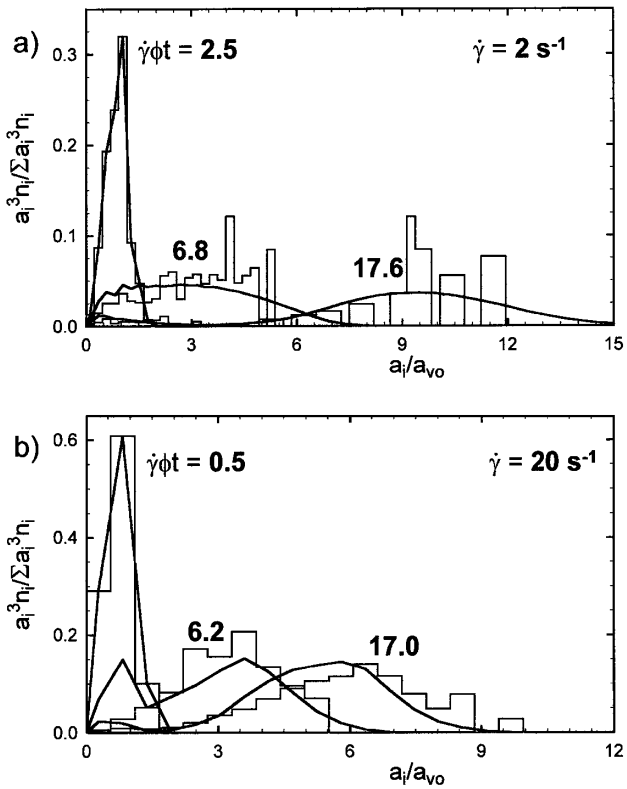

FIG. 4. Dimensionless drop-size distribution at different dimensionless times for the data of Fig. 3 at a shear rate of (a) 2 s^{-1} and (b) 20 s^{-1}. The stepped histograms are the measured distributions, and the solid curves are the predicted distributions from Ref. [10].

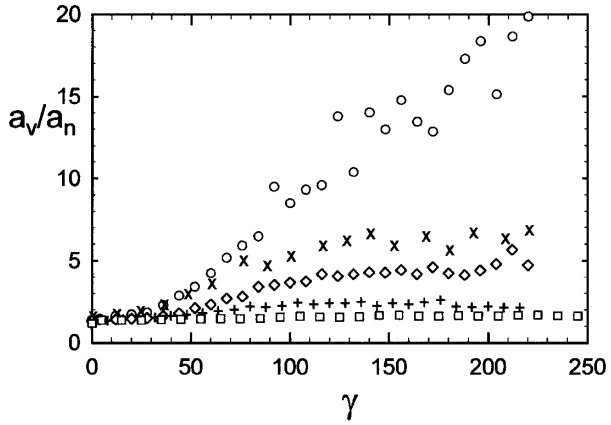

FIG. 5. Evolution of the drop-size polydispersity index a_v/a_n for shear rates of 2, 5, 10, 20, and 50 s^{-1} from top to bottom.

small drops. This result agrees quantitatively with the predicted value [9] of $\varepsilon = 0.56$ for spherical drops, $p = 0.2$, and $k = 1$. Indeed, we expect the experimental value of ε to be dominated by that for equal-sized drops (i.e., $k = 1$), since the volume average biases the largest drops, and the most significant growth is caused by collisions with drops of equal size. Even so, theoretical values [9] of ε do not decrease significantly until k is much less than unity (i.e., less than 0.5): e.g., $\varepsilon(k = 0.7) = 0.55$, $\varepsilon(k = 0.5) = 0.48$, and $\varepsilon(k = 0.3) = 0.36$. Since the viscosity ratio is essentially independent of temperature, ε for spherical drops is the same at each of the temperatures studied.

After the drops achieve a certain size, which is smaller for faster shear rates, ε sharply decreases due to a slow film-drainage process [10,19], and the growth curve bends over, consistent with drops being deformed at the point of their apparent contact. The curved lines (Fig. 3) are generated from Rother and Davis' theory [10] using the Hamaker parameter ($A = 10^{-19}$ J) as the single fitting parameter. This value of the Hamaker constant is reasonable, though perhaps in the upper end of the range of expected values [20].

Drop deformation is influenced by temperature, because of changes in viscosity and interfacial tension. The change in viscosity is more significant (Table I), so that the onset of drop deformation (and the sharp reduction in ε) occurs at smaller drop size when the temperature is lower.

The reduction in ε for large-sized drops also has a significant influence on the drop-size distribution. When the drops are small enough that they remain spherical, coalescence is most likely between drops of similar size [9], and the distribution broadens significantly [21], as observed especially at the lower shear rates for which deformation is less important (Fig. 4a). At high shear rates (Fig. 4b), drop growth is less, and the size distribution does not broaden as much, because of the reduction in ε especially of the large drops due to small deformation and film drainage in the near-contact region [10]. Good agreement between theory and experiment is observed. Additional data demonstrating that much narrower distributions are achieved at higher shear rates are provided in Fig. 5 as a plot of the drop-size polydispersity index versus strain.

The authors gratefully acknowledge the financial support of NSF Grant No. CTS-9731502 and NASA Grant No. NAG3-2116.

*Email address: steven.hudson@nist.gov

[1] X. G. Zhang and R. H. Davis, J. Fluid Mech. **230**, 479 (1991).
[2] M. J. Hadamard, C.R. Acad. Sci. Paris **152**, 1735 (1911).
[3] M. A. Rother, A. Z. Zinchenko, and R. H. Davis, J. Fluid Mech. **346**, 117 (1997).
[4] M. Smoluchowski, Z. Phys. Chem. **92**, 129 (1917).
[5] D. L. Swift and S. K. Friedlander, J. Colloid Sci. **19**, 621 (1964).
[6] H. Mousa and T. G. M. vandeVen, Colloids Surf. **60**, 19 (1991).
[7] A. Nandi, A. Mehra, and D. V. Khakhar, Phys. Rev. Lett. **83**, 2461 (1999).
[8] A. J. Ramic *et al.,* Macromolecules **33**, 371 (2000).
[9] H. Wang, A. Z. Zinchenko, and R. H. Davis, J. Fluid Mech. **265**, 161 (1994).
[10] M. A. Rother and R. H. Davis, Phys. Fluids **13**, 1178 (2001).
[11] A. Saboni, C. Gourdon, and A. K. Chesters, J. Colloid Inferface Sci. **175**, 27 (1995).
[12] A. Luciani, M. F. Champagne, and L. A. Utracki, J. Polym. Sci. Polym. Phys. Ed. **35**, 1393 (1997).
[13] C. Huh and S. G. Mason, Colloid Polym. Sci. **253**, 566 (1975).
[14] *Labview IMAQ Vision Handbook* (National Instruments Corp., Austin, TX, 1996), p. 71.
[15] T. Imaeda, Physica (Amsterdam) **285A**, 306 (2000).
[16] M. Loewenberg and E. J. Hinch, J. Fluid Mech. **338**, 299 (1997).
[17] F. R. daCunha and E. J. Hinch, J. Fluid Mech. **309**, 211 (1996).
[18] S. D. Hudson and P. V. Gopalkrishnan (to be published).
[19] A. K. Chesters, Chem. Eng. Res. Des. **69**, 259 (1991).
[20] M. E. Schimpf and S. N. Semenov, J. Phys. Chem. B **104**, 9935 (2000).
[21] S.-P. Lyu, F. S. Bates, and C. W. Macosko, AIChE J. **46**, 229 (2000).